JOURNAL OF MATERIALS SCIENCE 31 (1996) 4655–4661

Fine-scale morphology of ultraviolet–ozone etched polyethylene

S. HERBERT, D. M. SHINOZAKI
Department of Materials Engineering, The University of Western Ontario, London, Ontario, Canada, N6A 5B9
R. J. COLLACOTT
Dow Chemical Canada Inc., Sarnia, Ontario, Canada, N7T 7M1

The process of ablation of the surface of polyethylene using ultraviolet radiation in the presence of ozone has been studied. The average rate of material erosion is quite small but is selective, preferentially etching the amorphous regions. The resultant fine scale surface topography has been examined using transmission electron microscopy of replicas, and lamellae are readily visible. The light source emitted two principal wavelengths, with the shorter wavelength affecting measured etching rates more strongly.

1. Introduction

It is well known that organic polymers are sensitive to ultraviolet (UV) radiation [1], and are also degraded in the presence of ozone. The combination of the two has been reported to accelerate degradation processes [2]. Ozone can be produced from molecular oxygen irradiated with UV of wavelengths shorter than 242 nm [3]. Hence illumination of a polymer surface, with short wavelength UV in the presence of air generates ozone at the polymer surface, which together with the UV causes rapid ablation of the polymer specimen. The reported rates of removal of thin hydrocarbon contamination layers deposited on synchrotron optical components [4], suggested that such a technique may be useful as an etching method to reveal lamellar microstructure in polyethylene. In addition, there is some interest in using such techniques to clean semiconductor surfaces [5] and to modify polymer surfaces chemically as a preparation for subsequent processing [6].

Other techniques used to attack polyethylene include the use of ozone for selective degradation of single crystals [7] and the standard permanganic acid etch [8]. More recently, air plasma [9] and vacuum UV [10] have been applied. The purpose of the present work was to study the fine-scale morphology produced in high-density polyethylene subjected to UV–ozone etching.

2. Experimental procedure

Polyethylene (Sclair resin, Dupont, Canada) with a known large spherulite size was chosen for these experiments so that large-scale microstructural features could be clearly identified. The material had a density of 0.96 $g\,cm^{-3}$ and was compression moulded from pellets at 205 °C and slowly cooled. The spherulite diameter was typically about 50 μm and appeared banded under the optical microscope. Polyethylene of varying octene co-monomer content was obtained from Dow Chemical Canada Inc.. Nominal density values for these polyethylenes ranged from 0.875–0.945 $g\,cm^{-3}$. These materials were used to study the effect of the crystalline-amorphous phases on the etching behaviour.

Differential scanning calorimetry (DSC) data were generated on a TA Instrument TA2200 thermal analysis system equipped with a TA2910 DSC module. Calibration was done with indium metal standard with the heat of fusion and onset of melting control charted and in statistical control. The 3σ values were ± 0.2 °C and $\pm 0.9\,J\,g^{-1}$, respectively. A HDPE standard was control charted to determine technique reproducibility; 3σ values were 130.9 ± 0.5 °C and $218 \pm 17\,J\,g^{-1}$.

All polyethylene samples were conditioned to the same thermal history (200 °C for 2 min then cooled at 10 °C min^{-1} to 25 °C). The sample stood for 24 h prior to analysing to ensure completion of latent crystallization. The thermal curve data was taken at 10 °C min^{-1} from 0–200 °C. Helium was used as a purge gas at a flow rate of 50 ml min^{-1}. Per cent crystallinity was calculated using a heat of fusion value of 293 $J\,g^{-1}$ for pure crystalline polyethylene.

The compression-moulded samples were etched at varying distances from a fused quartz low-pressure mercury vapour lamp. Such lamps produce wavelengths of 185 and 254 nm. The light source was in the form of a flat grid with an area of approximately 5 cm × 15 cm. The source cross-sectional dimensions were much larger than the source to specimen distance. The sample and source were contained in a glass bell jar with a slow circulation of air pumped into the bell jar.

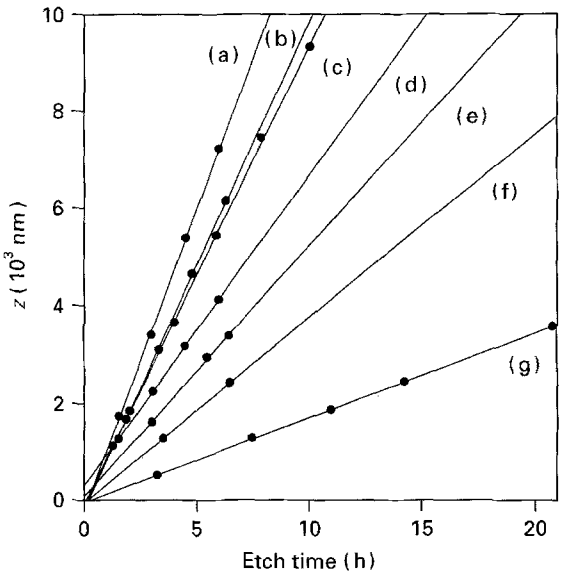

Figure 1 Depth of etching as a function of time for increasing sample to source distances: (a) 0.300, (b) 0.825, (c) 1.295, (d) 1.765, (e) 2.245, (f) 3.195, (g) 5.095 cm.

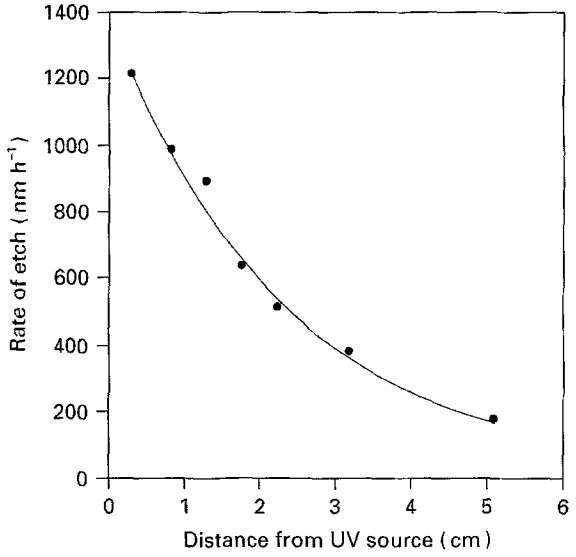

Figure 2 Rate of etching versus sample to source distance.

The compression-moulded surface was etched in one set of experiments. Most of the etching was performed on surfaces cut with a steel blade in a plane normal to the compression-moulded face.

The changes in mass of the specimen were measured using a microbalance which allowed measurements to a precision of $\pm$ 0.002 mg.

Two-stage replicas for transmission electron microscopy were prepared using a standard method. Cellulose acetate softened in solvent was pressed on to the etched surface, dried and removed. The replica was shadowed with a thin layer of AuPd in a vacuum evaporator at a nominal angle of 15°–30° with respect to the surface. This was backed by approximately 40 nm carbon, also vacuum evaporated. The cellulose acetate was dissolved carefully in a solvent, and the metal-shadowed carbon replica deposited on a grid. These were then examined in a Jeol 100CX transmission electron microscope (TEM) using an operating voltage of 80 kV.

3. Results and discussion

3.1. Mass loss measurements

The mass loss resulting from progressive UV–ozone attack was measured for increasing sample to source distances, starting at 0.30 cm. Assuming the mass loss was entirely from the surface facing the source, and knowing the area of the exposed face, the measured mass loss could be converted to an average decrease in thickness. The average loss in thickness increases linearly with exposure time, with rates of attack increasing with decreasing source to sample distance (Fig. 1). The plotted lines in Fig. 1 represent linear regressions which fit very well to the data.

The rate of thickness loss averaged over the exposed surface showed an exponential decay with distance (Fig. 2), and the curve fitted to a function of the form

$$\frac{dz}{dt} = 1.38 \times 10^4 \exp(-0.422z) \quad (1)$$

where z is the source to sample distance and t is time (h).

The form of the function suggests that the rate of ablation of the sample is proportional to the intensity of radiation at the sample surface. This intensity decreases exponentially with increasing absorption path length according to the simple Lambert–Beer function

$$I = I_0 \exp(-\mu z) \quad (2)$$

where I is the intensity of the radiation after passing through a medium of thickness z with an absorption coefficient μ. The intensity at the source is I_0.

The experimental data were also fitted to a sum of two exponentials; a functional form is expected if the two principal wavelengths of 184.9 and 253.7 nm radiation were in combination affecting the rate of ablation. The second exponential term is effectively insignificant, indicating the predominant influence of one wavelength in the ablation process.

The two wavelengths from the lamp are both needed to produce the rapid ablation rates. The 185 nm light dissociates molecular oxygen to produce ozone. The longer wavelength initates decomposition of the ozone to counterbalance the generation of the gas [3]. At the specimen surface, valence electronic excitation is predominant at wavelengths longer than 200 nm, and photo-ionization becomes predominant below 150 nm [1]. The shorter wavelength is thus expected to generate significant amounts of chain scission in the polyethylene. Ozone, of course, reacts strongly with carbon double bonds in rubber. it also reacts with polyethylene to form free radicals, which in turn oxidizes the polymer. The rapid mass loss measured shows that volatile compounds are formed.

Vig [2] presents empirical data which show that the most rapid mass loss in thin organic contamination layers on quartz occurs in the presence of the radiation of the two principal wavelengths with ozone. Interpretation of his data suggests that the 185 nm

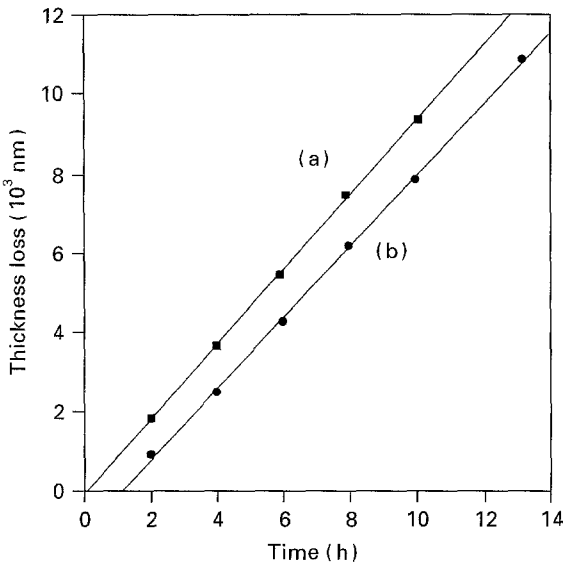

Figure 3 Incubation time of approximately 1 h for etching as-moulded surfaces (b) compared to a previously etched surface (a). Sample to source distance = 1.30 cm.

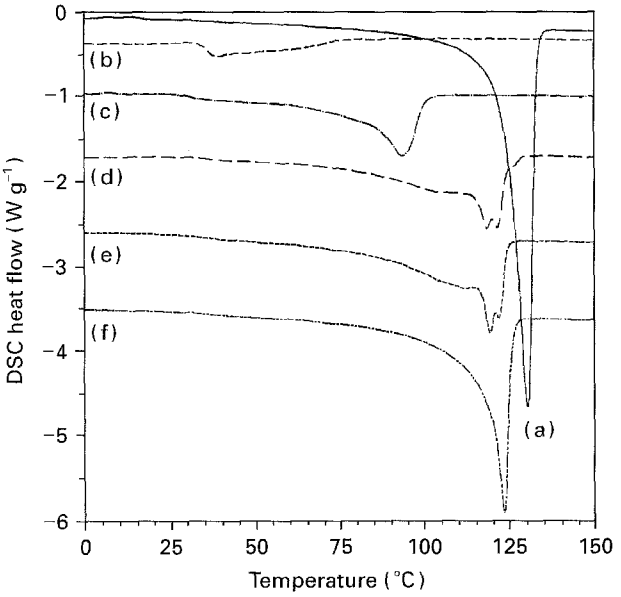

Figure 4 DSC thermal curves for five ethylene–octene co-polymers. (a) 0.950, (b) 0.875, (c) 0.905, (d) 0.915, (e) 0.920, (f) 0.930 g cm^{-3}.

radiation is more important in accelerating the organic mass loss. This is consistent with the observations made here in polyethylene, in which the mass loss is principally affected by the 185 nm radiation.

It is possible to estimate the concentration of ozone using the data in Fig. 2. The published total photoabsorption cross-sections for 185 nm radiation show that ozone is many orders of magnitude more absorbing than is oxygen [11] and presumably also to nitrogen. Very small concentrations of ozone would affect the intensity at the specimen surface. Calculation of the relative amounts of ozone compared to oxygen show that about 2–3% of the molecules in this region between the source and the specimen are ozone molecules.

In Fig. 2 the datum at the distance of 1.3 cm lies above the exponential curve fitted to all data. Repeated experiments around this distance show that this discrepancy is a reproducible experimental result, and is statistically significant. The interpretation of this result is not clear, but is likely related to the coupling of the UV irradiation damage processes and the concentration of ozone at the reactive surface of the sample.

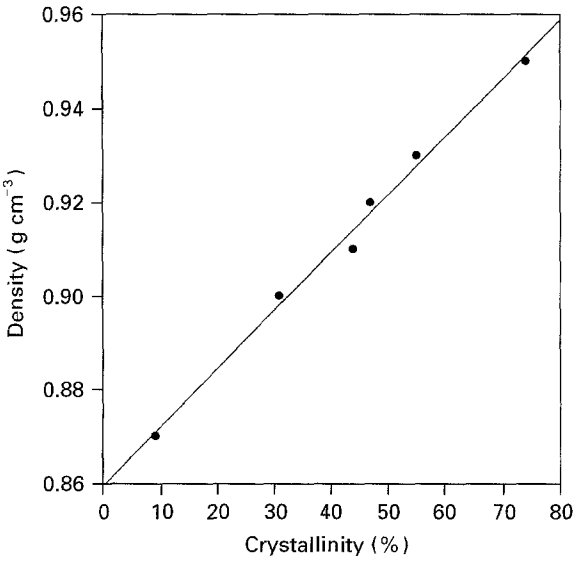

Figure 5 Density as a function of crystallinity for the different resins.

3.2. Microstructural effects

The plots of the mass loss versus time of etching could be used to reveal the presence of a surface layer or "skin" on as-moulded specimens. Fig. 3 shows the data compared for two specimens. The first set of results is for a compression-moulded sample, in which the moulded surface is etched. The second set of results is for a similarly compression-moulded sample in which the moulded surface layer has been previously etched away. The pre-etched sample shows a linear regression which extrapolates back through the origin. The as-moulded sample shows a shift to higher times. The two samples etch at the same rate, but the moulded sample has an incubation time of about 1 h before significant rates of ablation begin.

This would suggest that the microstructure at the surface, and its susceptibility to etching are different from the bulk. From the incubation time measured, the thickness of this surface "skin" appears to be approximately 0.9 μm. Such a layer would be difficult to observe using most standard methods of microstructural examination. The surface layer is unlikely to be chemically distinct from the bulk, but may be microstructurally different because of the thermal gradients generated during solidification. The direction of the shift in ablation rates is surprising in view of the results discussed later, in which amorphous polyethylene etches considerably faster than does the crystalline phase. The surface layer will cool more rapidly than the interior, and thus may have a lower crystallinity than the interior.

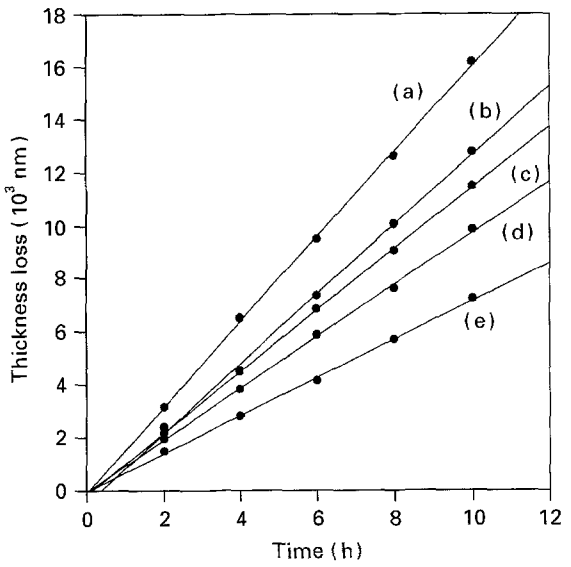

Figure 6 Depth of etching versus time for different crystallinities: (a) 9%, (b) 31%, (c) 44%, (d) 55% and (e) 74%. Sample to source distance = 0.87 cm.

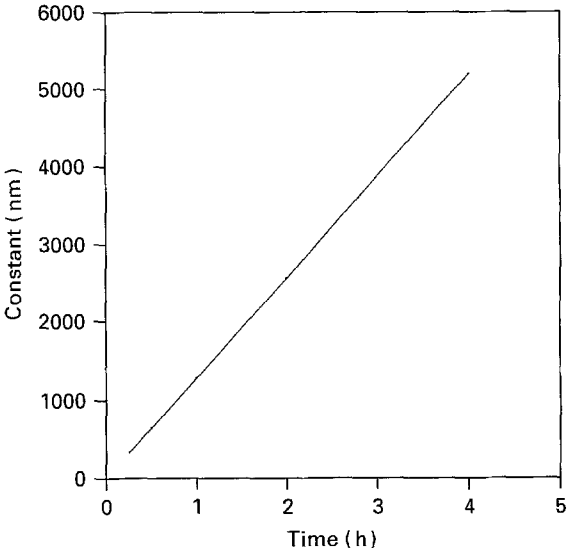

Figure 8 Contrast of crystalline–amorphous structure assuming no lateral etching. The contrast is defined as the etched depth difference between the two phases.

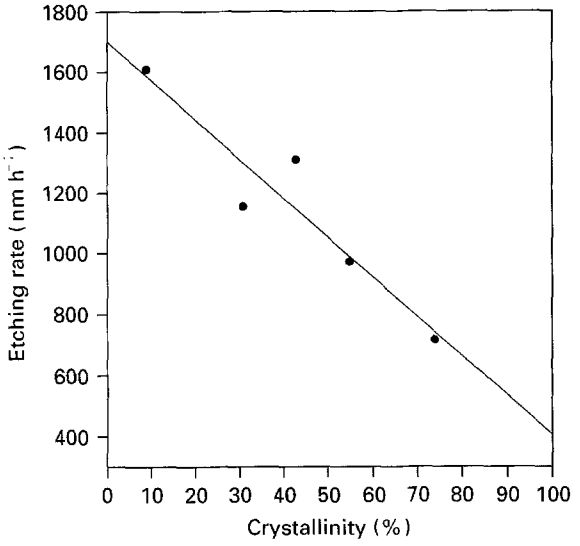

Figure 7 The linear dependence of the rate of etching on crystallinity.

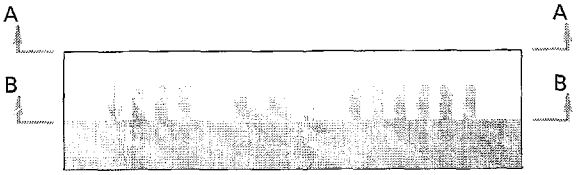

Figure 9 Schematic diagram of the topographic contrast developed with etching.

3.3. The effect of crystallinity

The differential scanning calorimetry (DSC) scans of the samples showed the expected increase in peak area with increasing crystallinity (Fig. 4). The density of the different materials decreased linearly with decreasing crystallinity as expected (Fig. 5). Rates of ablation were plotted versus sample crystallinity (Fig. 6). The rates were constant with time, and systematically increased with decreasing crystallinity. The data plotted are for previously etched surfaces, and no incubation times is observed. The incubation time before rapid ablation commenced was observed for as-moulded specimens for each crystallinity.

The rate of etching of the surface decreased linearly with mass fraction of crystallinity (Fig. 7) for a fixed specimen to source distance. This is expected in a simple model of etching of a two-phase (crystalline–amorphous) material. For a two-phase microstructure, the areal fraction of one phase exposed on the etched surface is equal to the volume fraction. If the two phases etch at different rates the average rate is weighted according to the areal fraction of each phase, and the linear relationship of Fig. 7 is expected.

3.4. Etched microstructures

In Fig. 7, the etch rates for the pure crystalline and pure amorphous phases can be estimated. For a two-phase crystalline–amorphous structure, the average height difference between the amorphous and crystalline phases after etching for different times can be approximated. This average peak to valley height difference is a measure of the topographic contrast in the etched surface (Fig. 8). This predicted contrast does not take into account the different rates of etching for different crystallographic orientations, which is discussed in the following section. Nor does the predicted contrast account for the etching which occurs laterally on protruding peaks in the topography. At long etching times, the lateral etching rates would erase high aspect ratio etched structures (Fig. 9). Hence small structures, such as edge-on lamellae, would best be observed after short etching times. Furthermore, in order to resolve the lamellae at short etching times, the surface must be prepared with as little deformation and damage as possible.

The resolution of microstructure typical of the bulk finally will depend on removing the surface layer of material which apparently has a different microstructure. This will require etching for at least 1 h.

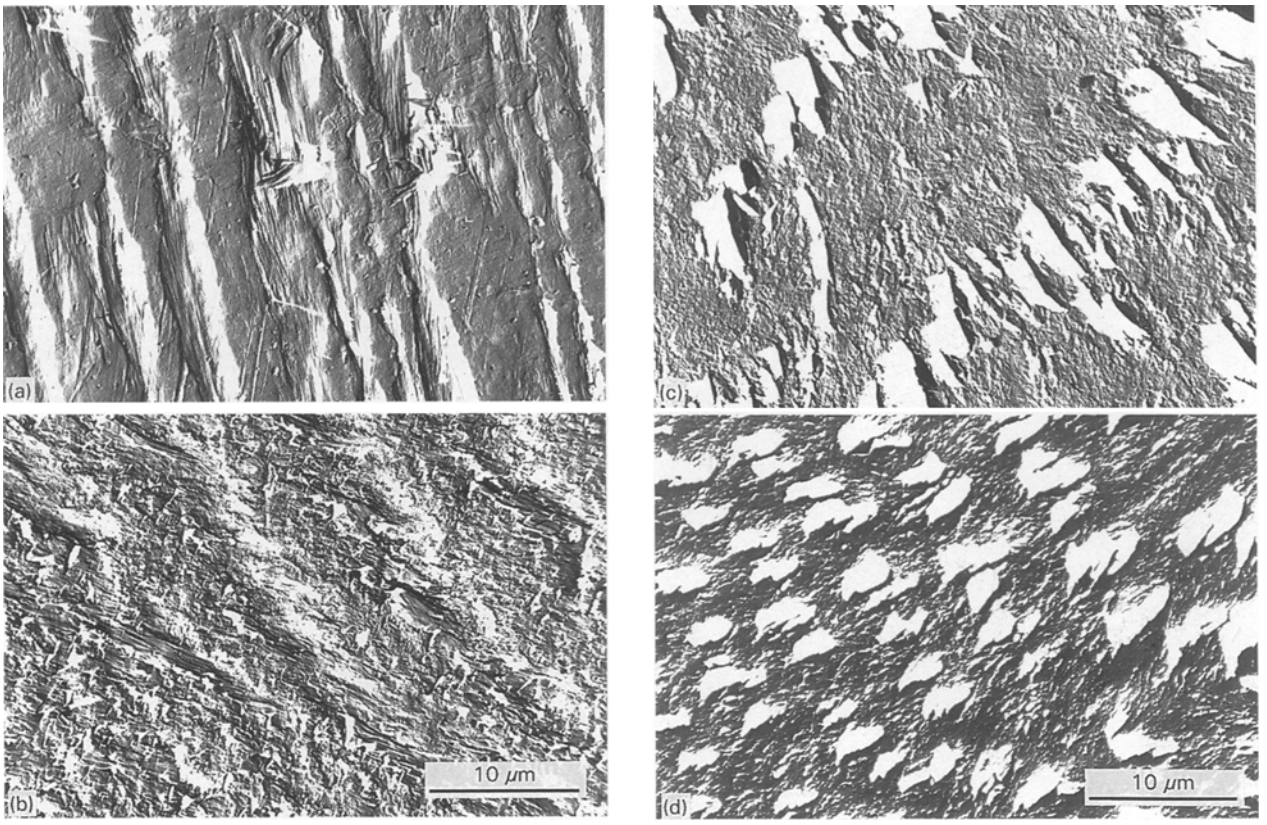

Figure 10 Low-magnification transmission electron micrographs of replicas. The original samples have been etched for increasing lengths of time: (a) no etch, cut marks are visible; (b) 30 min, (c) 2 h, the banded spherulitic structure is visible; (d) 4 h.

3.5. Morphology of etched surfaces

A surface cut from a compression-moulded sample is shown in Fig. 10. The cut marks are clearly visible, and the plastic deformation associated with the cut obscures any underlying microstructure. The replicas show topographic structure to scales of approximately 10 nm over large areas of the TEM specimen. The progressive evolution of the surface topography with increasing exposure to the UV–ozone etching is shown in Fig. 10b–d; the areas shown are typical of each sample.

After 30 min exposure (Fig. 10b), the original cutting marks are only slightly visible. This microstructure originates from a surface etched back an average distance of 417 nm from the original cut surface. With a total of 2 h etching, the periodic banded structure, evident in optical micrographs, is visible. The banding arises from the coherent twisting of the lamellae growing outwards from the spherulite centre. The large white areas observed correspond to regions where the lamellae are oriented parallel to the surface. The replicas show high electron transmission (white in these micrographs) in those areas with no AuPd coating. Hence these areas are in the shadow region of the AuPd evaporation step and are therefore much lower on the original etched surface. It is thus clear that the rate of ablation of the polyethylene lamellae is strongly orientation dependent, being considerably faster for the regions in which the lamellae lie flat and the lamellar normal is parallel to the direction of etching.

It is further expected from the etching rate-crystallinity dependence (Fig. 7) that amorphous regions would etch faster than the crystalline regions. Evidence for this is seen in Fig. 10c, in which specimens etched for 2 h show regions of lamellae etched edge-on. The spacing between successive dark lines in

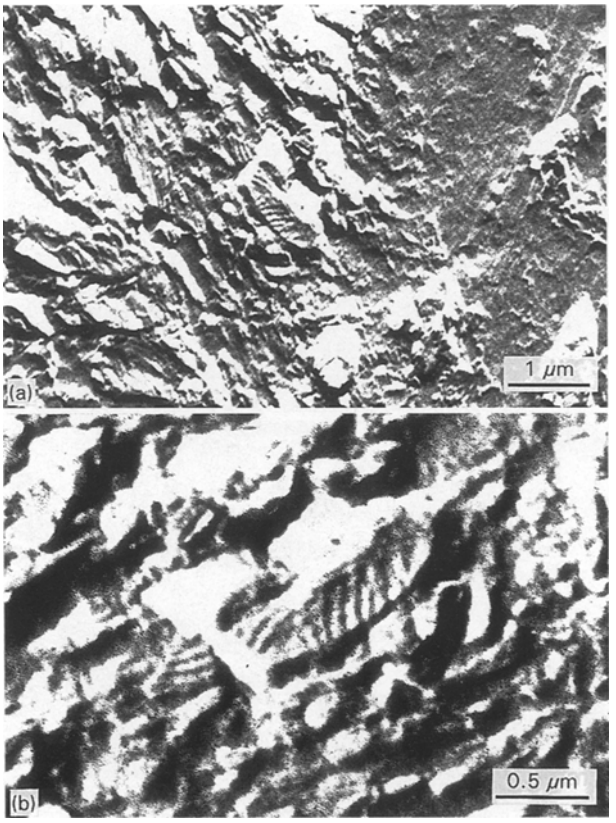

Figure 11 High-magnification images showing periodic structures with spacings similar to those expected for lamellae.

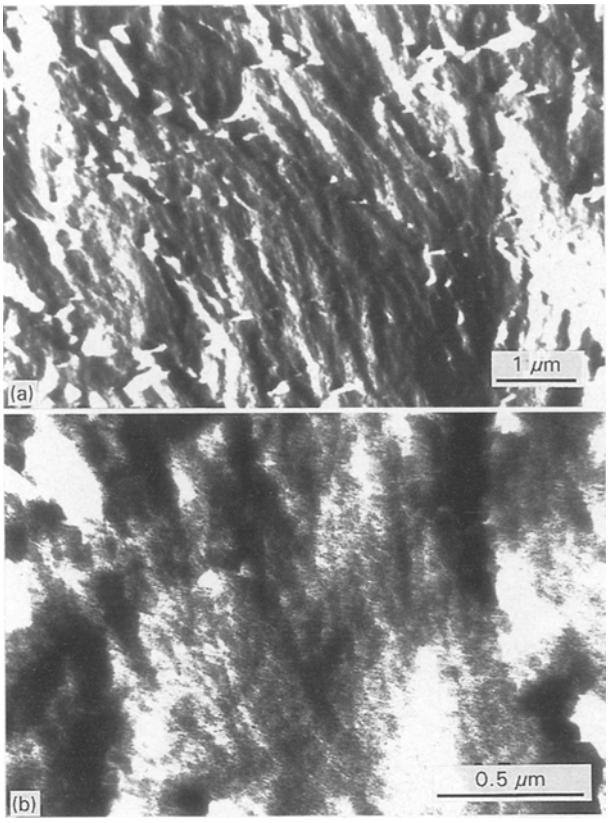

Figure 12 Long, edge-on lamellae visible only faintly (1 h etch with no xylene wash).

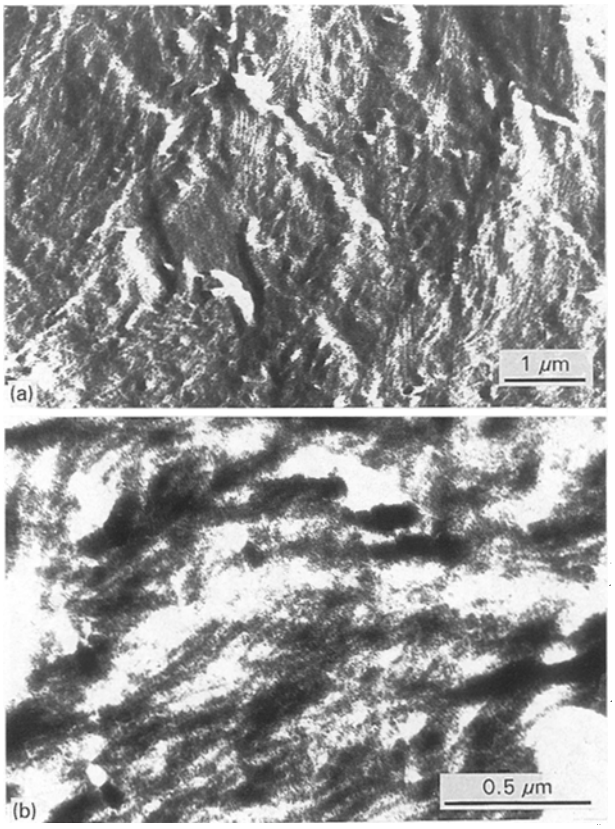

Figure 13 Lamellae are much more visible after washing in xylene (etching similar to Fig. 12).

Fig. 10c is approximately 30 nm. Higher magnification of selected areas reveals more clearly these lamellar structures (Fig. 11). Fig. 11b shows the width of the lamellae to be about 40 nm. These measured widths will depend on the orientation of the lamellae with respect to the etched surface.

Washing in xylene after exposure enhances the images at high magnification. The lamellae are more easily observed over larger areas of specimen. This can be seen by comparing high-magnification images of the replicas for specimens not washed in xylene (Fig. 12) with specimens washed in xylene (Fig. 13). Sadler and Keller [12] reported that low molecular weight polyethylene is selectively removed by washing in xylene at 35 °C. The UV irradiation of the surface is expected to cause chain scission and a reduction of molecular weight. The improvement in lamellar contrast seen on washing in xylene suggests there is a significant difference in UV-generated radiation damage rates in the crystalline and amorphous phases.

The improvement in lamellar resolvability with xylene washing is observed only after approximately 1 h UV–ozone etching. At shorter times (for example at 15 and 30 min), no lamellar image enhancement is found. This is consistent with the earlier observation of a surface skin (Fig. 3) which is effectively removed after approximately 1 h etching.

It appears that the explanation consistent with all experimental observations (visibility of lamellar periodicity, reduced etching rates within the 1 μm surface layer, and relative etching rates of lamellae oriented in different directions) is that the surface layer consists of lamellae oriented with their normals lying in the plane of the surface, but with an interlamellar spacing smaller than can be resolved with this technique (less than 20 nm).

4. Conclusion

Transmission electron microscopy of replicas of polyethylene etched under a UV–ozone source has revealed the fine-scale morphology. Lamellae can be resolved, although not as clearly as seen elsewhere with permanganic etching. The rates of mass loss have been measured and found to increase with decreasing crystallinity, and to depend on the crystallographic face exposed to the radiation. The 185 nm wavelength UV appears to be the most important component in determining ablation rates, being principally responsible for the chain scission and for the formation of ozone at the surface.

Acknowledgements

The funding for this project was principally from the Ontario Centre for Materials Research. The electron microscopy was assisted by Mr Don Gibson of the Department of Pathology at the University of Western Ontario.

References

1. J. GUILLET, "Polymer photophysics and photochemistry" (Cambridge University Press, Cambridge, 1985).

2. J. R. VIG, in "Treatise on clean surface technology", Vol. 1, edited by K. L. Mittal (Plenum Press, New York, 1987).
3. N. GRASSIE and G. SCOTT, "Polymer degradation and stabilization" (Cambridge University Press, Cambridge., 1985).
4. R. HANSEN, M. BISSEN, D. WALLACE, J. WOLSKE and T. MILLER, *Appl. Optics* **32** (1993) 4114.
5. S. PEARTON, F. REN, C. ABERNATHY, W. HOBSON and H. LUFTMAN, *Appl. Phys. Lett.* **58** (1991) 1416.
6. R. BRADLEY, I. CLACKSON and D. SYKES, *Appl. Surf. Sci.* **72** (1993) 143.
7. D. PRIEST, *J. Polym. Sci.* **9 (A-2)** (1971) 1777.
8. R. OLLEY and D. BASSETT, *Polymer* **23** (1982) 1707.
9. T. OGITA, A. PONOMAREV, S. NISHMOTO and T. KAGIYA, *J. Macromol. Sci. Chem.* **8** (1985) 1135.
10. W. KESTING, T. BAHNERS and E. SCHOLLMEYER, *J. Polym. Sci.* **31** (1993) 887.
11. R. DITCHBURN and P. YOUNG, *J. Atmos. Terr. Phys.* **24** (1962) 127.
12. D. SADLER and A. KELLER, *Koll. Z. Z. Polym.* **242** (1970) 1081.

Received 31 October 1994
and accepted 28 April 1995